Cassini Imaging of Jupiter's Atmosphere, Satellites, and Rings

Carolyn C. Porco,[1]* Robert A. West,[2] Alfred McEwen,[3] Anthony D. Del Genio,[4] Andrew P. Ingersoll,[5] Peter Thomas,[6] Steve Squyres,[6] Luke Dones,[1] Carl D. Murray,[7] Torrence V. Johnson,[2] Joseph A. Burns,[6] Andre Brahic,[8] Gerhard Neukum,[9] Joseph Veverka,[6] John M. Barbara,[4] Tilmann Denk,[10] Michael Evans,[1] Joseph J. Ferrier,[4] Paul Geissler,[3] Paul Helfenstein,[6] Thomas Roatsch,[10] Henry Throop,[1] Matthew Tiscareno,[3] Ashwin R. Vasavada[11]

The Cassini Imaging Science Subsystem acquired about 26,000 images of the Jupiter system as the spacecraft encountered the giant planet en route to Saturn. We report findings on Jupiter's zonal winds, convective storms, low-latitude upper troposphere, polar stratosphere, and northern aurora. We also describe previously unseen emissions arising from Io and Europa in eclipse, a giant volcanic plume over Io's north pole, disk-resolved images of the satellite Himalia, circumstantial evidence for a causal relation between the satellites Metis and Adrastea and the main jovian ring, and information on the nature of the ring particles.

The Cassini spacecraft was launched in October 1997 and, en route to Saturn, encountered Jupiter in December 2000. During this event, the Cassini Imaging Science Subsystem (ISS), the highest resolution two-dimensional imager on the Cassini orbiter (*1*), collected ~26,000 images of Jupiter, its satellites, and its rings. Scientific objectives at Jupiter included investigation of its three-dimensional cloud structure, global meteorology, and auroras; imaging of known satellites, especially during eclipse; searching for previously unseen satellites; and determining the structure, particle properties, and temporal variability of the jovian rings.

[1]Department of Space Sciences, Southwest Research Institute, 1050 Walnut Street, Suite 400, Boulder, CO 80302, USA. [2]Jet Propulsion Laboratory, California Institute of Technology, 4800 Oak Grove Drive, Pasadena, CA 91109, USA. [3]Department of Planetary Sciences, University of Arizona, 1629 East University Boulevard, Tucson, AZ 85721, USA. [4]Goddard Institute for Space Studies, NASA, 2880 Broadway, New York, NY 10025, USA. [5]Division of Geological and Planetary Sciences, California Institute of Technology, 150-21, Pasadena, CA 91125, USA. [6]Department of Astronomy, Cornell University, Space Sciences Building, Ithaca, NY 14853, USA. [7]Astronomy Unit, Queen Mary, University of London, London E1 4NS, UK. [8]Centre d'Etudes de Saclay, University of Paris, L'Orme des Merisiers, 91191 Gif-sur-Yvette Cedex, France. [9]Department of Earth Sciences, Freie Universität, 12249 Berlin, Germany. [10]Institute for Space Sensor Technology and Planetary Exploration, German Aerospace Center, Rutherfordstrasse 2, 12489 Berlin, Germany. [11]Department of Earth and Space Sciences, University of California, Los Angeles, CA 90095, USA.

*To whom correspondence should be addressed. E-mail: carolyn@ciclops.swri.edu

The Cassini Jupiter flyby was slow and nearly equatorial (*1*). Data collection began on 1 October 2000 with the spacecraft 3.8° above Jupiter's equatorial plane and approaching the planet from a phase (Sun-Jupiter-spacecraft) angle of 20° and a distance of 84.7 million km. By the middle of December, the phase dropped to 0°, and the spacecraft began a month-long sweep through a large range of phase angles. By 15 January 2001, the spacecraft was on an asymptotic trajectory out of the jovian system, looking back on a crescent Jupiter from a distance of 18 million km, a phase angle of 120°, and an elevation of 3° below the plane of the equator. The last Jupiter images were taken on 22 March 2001.

Cassini's closest approach distance to Jupiter's cloud tops (30 December 2000, 10:05 UTC) was 136 jovian radii R_J, or 9.72 million km, and resulted in an image scale in the narrow-angle camera (NAC) of 58 km/pixel. Thus, Cassini images did not have the exquisitely high resolution of Voyager and Galileo images. However, the long duration of the flyby, the large data storage capacity and high transmission rate of the spacecraft, and the photometric sensitivity, linearity, spectral range, and numerous data collection modes of the ISS (*2*) made it possible to acquire many high-quality time-lapse images of Jupiter's changing atmosphere between 1 October 2000 and 22 March 2001 and to image dynamic processes within the jovian satellite and ring systems.

Jupiter's atmosphere. The lengthy 6-month baseline of Cassini Jupiter observations and the wide spectral range of the ISS from the ultraviolet (UV) into the near-infrared (near-IR) were critical for discriminating Jupiter's multilevel clouds, aerosols, and hazes and for monitoring the evolving cloud structures and winds that reveal underlying atmospheric dynamics and chemistry (*1*). The stability of Jupiter's zonal winds, given the turbulent nature of its cloud patterns, is a remarkable feature of its atmosphere. Nonetheless, the zonal wind profile as observed by the ISS (*3*) (Fig. 1) shows small changes in the shape and speed (less than or equal to ~40 m/s) of some of the zonal jets, as compared to those observed by Voyager (*4*), consistent with recent analyses from Galileo and the Hubble Space Telescope (HST) (*5*–*7*). It also reveals polar jets in each hemisphere that were not previously detected in the visible-wavelength Voyager data. Toward the polar regions in each hemisphere, the banded patterns that characterize Jupiter's appearance gradually give way to a seemingly chaotic pattern of hundreds of interacting vortices. However, Cassini movies of the jovian atmosphere reveal that near the poles, as at lower latitudes, the

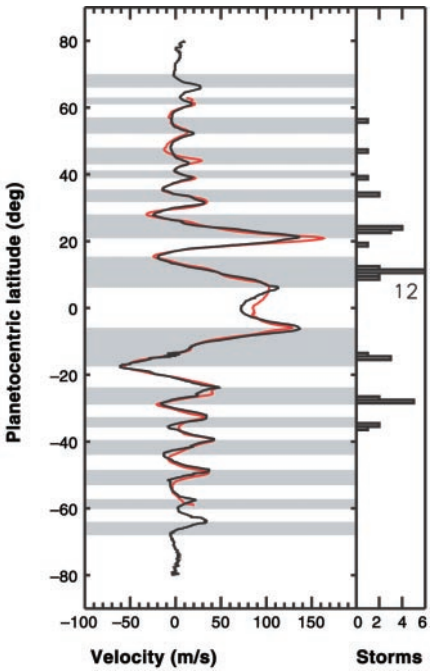

Fig. 1. (**Left**) The black line is the average of wind speeds measured with an automatic correlation technique on 29 pairs of Cassini images separated by 10 hours (*3*); the red line is derived from Voyager 2 images (*4*). The eastward jet at 23°N has slowed from 180 to 140 m/s. The westward jet at 30°N and the jets between 40° and 55°N also show changes of 10 to 20 m/s and small shifts in latitude. (**Right**) Latitudinal distribution of convective feature occurrence. Latitudes are estimates in planetocentric coordinates obtained by visually mapping a grid to the limb. Estimated accuracies are ~1° near the equator and degrade with increasing latitude. Gray regions are belts; white regions are zones.

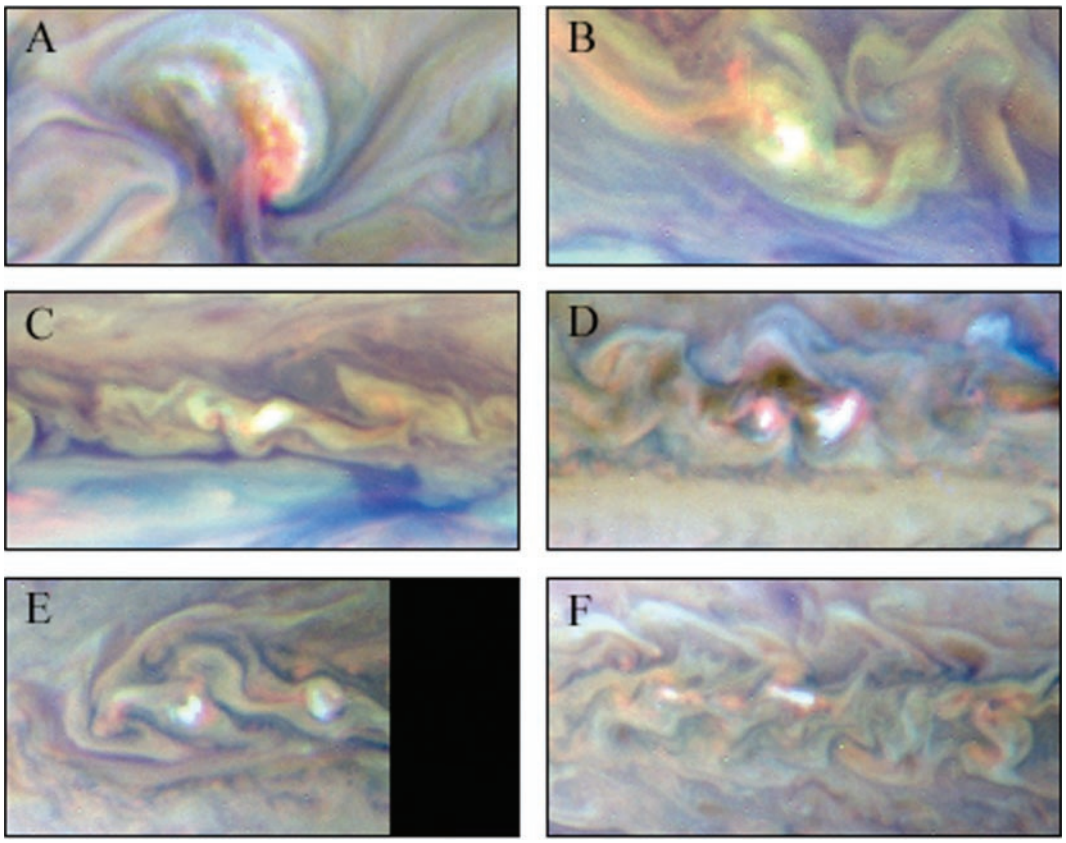

Fig. 2. False-color images of jovian convection. The continuum, weak methane, and strong methane images are loaded into the red, green, and blue color planes, respectively. Convective storms appear as small white regions. Spatial resolution was ~175 km in early December 2000 and ~60 km at the closest approach (30 December). Locations and dates are as follows: (**A**) 14°S, 29 December; (**B**) 10°N, 31 December; (**C**) 12°N, 2 December; (**D**) 23°N, 1 January 2001; (**E**) 34°N, 1 January; and (**F**) 35°S, 1 January. Storm dimensions sometimes exceed 2500 km (A) but are typically a few hundred km. Usually, storms are adjacent to regions with deeper clouds (red). Storms are most common in the North Equatorial Belt [(B) and (C)], but they also occur northwest of the Great Red Spot (A), poleward of the 23°N jet (D), and at higher latitudes [(E) and (F)]. Equatorial plume cores are not as optically thick as small convective storms in the same image (C). Much of their area is made up of optically thin high clouds [a region that is bright only in the strong methane band (turquoise)]. Away from the plume cores, sunlight penetrates deeper (the pink area at the bottom left) but not as deep as the regions near the small convective storms. The plumes may thus not be convection, but rather organized regions of less vigorous large-scale vertical motion. The storms in (E) fell near the edge of the image, explaining the "missing data" on the right.

vortices are long-lived (i.e., many survive the entire encounter period) (movie S1) and are transported around the planet by steady zonal jets. The polar vortices exhibit small irregular motions in latitude and longitude, but unlike the waves in the jet streams of Earth, the jovian high-latitude jets do not develop large-amplitude excursions in latitude. The presence of zonal jets at high latitudes may be an important discriminator between different models of Jupiter's interior structure and dynamics (*8–10*), although this matter is in dispute (*11*).

Observations from three near-IR ISS filters were used to detect convective clouds on Jupiter (*12*). Convective features appear in the dark bands in the jovian atmosphere (called "belts"), where they are brighter than surrounding cloud features (Fig. 2) (*1*); they are also brighter than any region in the adjacent bright bands (called "zones"), with the exception discussed below. Sometimes jovian storms last ~10 days, exceeding the lifetimes of terrestrial storms (Fig. 3). A deep stationary disturbance associated with the Great Red Spot must keep the atmosphere convectively unstable; this would explain how such features persist in the same location in the midst of a turbulent, rapidly changing local flow at the visible cloud top level.

The jovian belts are cyclonic shear zones (*13*). The tendency for convective storms (*14*), which are the source of jovian lightning, to occur in the belts (Fig. 1) is consistent with previous work (*15, 16*). Storms are typically a few hundred km in size, but occasionally can exceed 2500 km. The presence of such storms in the equatorial zone is ambiguous because the high, bright, and extensive cloudiness of the zone makes storm detection difficult. No convective storms, however, are detected in the other bright zones.

The convective interior of Jupiter and its visible cloud tops are connected through a process of deep moist convection (*17–19*), analogous to terrestrial storms that control the circulation and climate of Earth's tropics. Model simulations suggest that jovian deep convection, originating at the water condensation level at ~5 bars, can extend above the 500-mbar pressure level (*20, 21*). Lower convection heights are possible, depending on the properties of the air outside the clouds and the extent of mixing into the updrafts. If the large-scale visible cloud tops in the zones are ammonia clouds at 550 to 750 mbar (*18*), then weak convection might exist there but not penetrate the visible cloud top; thus, the convection might not be detected. On the other hand, if the visible clouds are primarily ammonium hydrosulfide with tops below the 1-bar level (*22, 23*), convection should penetrate much higher given the probable adiabatic lapse rates below 1 bar. In this case, the absence of convective detections in the zones would imply no convection there at any level.

Previous studies indicate that jovian lightning occurs preferentially at high latitudes (*15, 16*). However, we observed convective features more often at low latitudes (Fig. 1), even after accounting for the smaller observable area at high latitudes. It is possible that this discrepancy is due to a bias in viewing geometry or because of inadequate sampling. On the other hand, on Earth the geographic distributions of lightning and convection differ. Terrestrial lightning occurs primarily over land, where temperature lapse rates often exceed the moist adiabatic lapse rate and where updrafts are strong, whereas convection is frequent over the oceans but rarely produces lightning because lapse rates are nearly moist adiabatic and updrafts are thus weaker (*24, 25*). If temperatures deep within Jupiter are globally uniform, the differing latitudinal distributions of moist convection and lightning that we report here imply that temperature above the water condensation level decreases from the equator to mid-latitudes. This is consistent with observed latitudinal profiles of upper troposphere temperatures (*26*) and jovian weather layer models (*27*).

The zones and belts have been traditionally viewed as regions of large-scale upward and

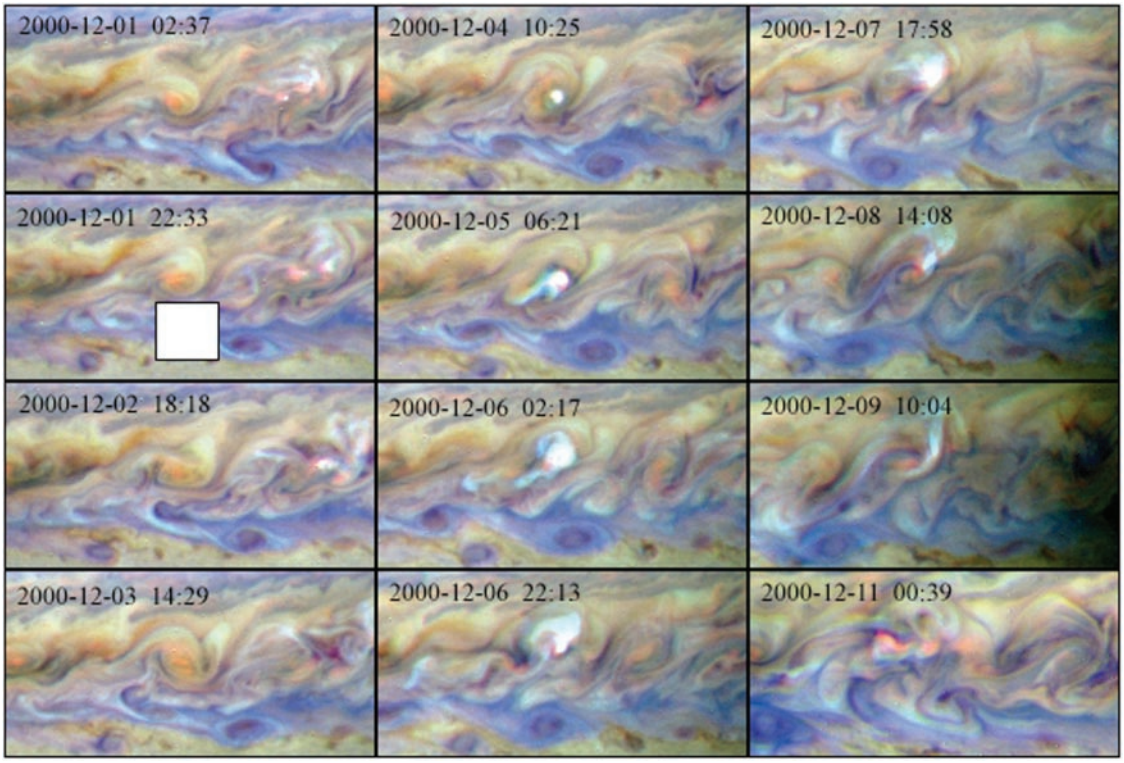

Fig. 3. Temporal evolution of a persistent convective storm region located northwest of the Great Red Spot at 14°S latitude during the period 1 to 11 December 2000. All times are UTC. Data missing from the second panel in the first column are due to the passage of the satellite Io across the jovian disk. On 1 December, a small convective cloud appeared near the right edge but disappeared 2 days later. At the same time, a deeper cloud was visible in the center of the image. On 4 December, deep convection was generated in this region. Over the next 5 days, it grew to ~2100 km and then was sheared out by the flow. A week after its appearance, it disappeared, and deeper clouds were again visible. On 11 December (not shown), the storm briefly reformed before disappearing.

downward motion, respectively (*17*). However, we observed vigorous convection restricted to the belts, which implies large-scale convergence and upward motion at depth, where water condenses (~5 bars), in the belts. To be consistent with the hot spots and generally lower cloud tops in the belts (*23*), the rising motion must be confined to the relatively small convective areas that we observed. Mass conservation would then suggest that the zones should be regions of moisture divergence and sinking motion at depth. Their cloudy appearance implies either a reversal of this vertical circulation pattern (i.e., rising motion) in the upper troposphere (*28*) or an analog to the subtropical marine stratocumulus regions on Earth, in which extensive cloudiness is maintained by moisture trapped between small-scale and weak upward turbulent mixing and the large-scale sinking motion from above (*29*).

One goal of the Cassini ISS investigation of Jupiter was an examination of its polar regions at all wavelengths, especially in the UV (*1*). For 2.5 months, from 1 October 2000 to mid-December 2000, we obtained 1263 NAC images of Jupiter in the ultraviolet UV1 filter (258 nm). Together with images taken in the blue (451 nm), they indicate the presence of a high-altitude polar aerosol that becomes rapidly more optically thick and more obscuring of the deeper clouds over a larger circumpolar area from the blue to the near-UV (*30*).

The UV1 images were acquired with sufficient frequency and resolution to permit the construction of a stratospheric movie (movie S2). Six UV1 polar mosaics from the movie are shown in fig. S3. Many features can be seen in this series of frames, and the full movie shows how these features move and change with time. (At the moment, we cannot distinguish between several alternative hypotheses for producing such features; that is, variations in chemical composition, particle properties, and/or particle abundance could produce contrast.) Numerous circumpolar waves were observed between 40°N and 60°N latitude. These cannot be seen in the visible and near-IR continuum images. Similar features have been seen in HST images at 890 nm (*31*), but they are probably stratospheric Rossby waves forced by differential zonal motion.

The character of the motion changes poleward of the 60°N latitude circle, where the atmosphere is more homogeneous with small-scale features, several thousand km in size, that form and evolve on ~10-day time scales. The most prominent feature in this region is a large dark oval, 28,000 km in longitude by 18,000 km in latitude (about the same size and shape as Jupiter's Great Red Spot) (Fig. 4). This oval formed during the early part of our observations (between early October and mid-November 2000), evolved, grew in size, moved eastward, developed a bright inner core, began to circulate clockwise (against the prevailing counterclockwise rotation of the circumpolar vortex), elongated and thinned, and finally extended southward of the 60° boundary (movie S2).

These observations, which captured what may be a complete life cycle of this feature,

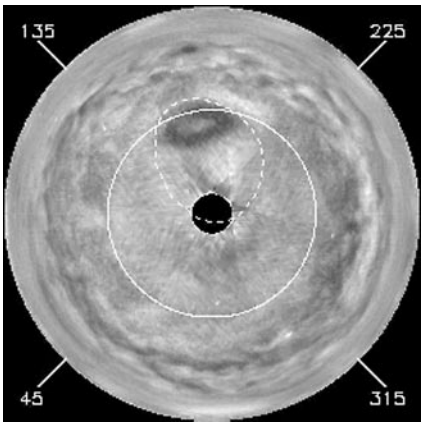

Fig. 4. The large dark oval observed in the middle of its life cycle (13 November 2000) in the northern jovian stratosphere in the UV (258 nm). The zero point of System III longitude is at the bottom of the image, and longitude increases in the clockwise direction. The 60°N latitude circle is shown. The location of the main auroral oval (*40*) is plotted as a dashed curve.

indicate that UV-absorbing haze on Jupiter may be used as a tracer of polar stratospheric motions. Other evidence suggests that large oval formation in the polar regions is a recurring phenomenon (*32, 33*), which may be quasi-periodic, or rare but recurring, and triggered by an unusual auroral event. For example, it is possible that the formation of polar stratospheric ovals may be linked to auroral precipitation. The most compelling evidence for this connec-

tion is the location of the large dark oval within the main auroral oval at the time when the former is at maximum contrast (Fig. 4). The alignment of the southern perimeter of the dark oval with the main auroral oval during that time suggests that the auroral process is contributing to the formation of the dark material, although its extension with time beyond the main oval weakens this interpretation. On time scales of weeks, auroral precipitation is a nearly continuous process along the main oval. The mechanism is thought to be tied to plasma corotation breakdown in the middle magnetosphere (*34*). A steady production of haze particles from this source might couple with unsteady flows in the upper atmosphere, resulting in a local concentration of particles. However, the evolution of the dark oval is currently unexplained.

Previous images of Jupiter at wavelengths sensitive to the high troposphere and stratosphere (*35, 36*) show that the planet is longitudinally homogeneous at low latitudes, except for contrasts associated with Jupiter's Great Red Spot and some smaller anticyclonic ovals that form high thick clouds. It was therefore surprising to see an obvious longitudinal wave of variations in both UV and near-IR brightness, with a crest-to-crest separation of ~22°, between 9° and 19°N (planetocentric) latitude, with a suggestion of the same wave in the cloud structures seen in the blue (Fig. 5). This region spans Jupiter's North Equatorial Belt and supports a large zonal wind shear in the troposphere (Fig. 1). At its southern boundary, the zonal flow is moving at 100 m/s, whereas at the northern boundary, the jet is retrograde with a velocity of –25 m/s (*37, 38*). The feature that is largest and brightest in the UV is centered near 0° longitude in System III, a longitude system that increases westward on the planet, is anchored to the rotation of the jovian magnetic field, and is the standard system for jovian atmospheric, auroral, and magnetic studies. Two or three other longitudes with enhanced brightness are apparent. (For reference, the System III longitude of the Great Red Spot in early October 2000 was ~33° and moving slowly westward.) Movies show these features to be nearly stationary in System III, but with brightness that varies with time.

Jovian stratospheric thermal waves have been seen with ground-based telescopes at a wavelength of 18.76 μm (*38*) and in thermal maps of Jupiter constructed from data obtained by the Cassini Composite InfraRed Spectrometer (CIRS) during the Jupiter flyby that occurred 2 to 4 weeks after the end of the ISS UV movie sequence (*39*). The ISS-observed brightness variations in the latitude band from 9° to 19°N appear to be correlated with temperature perturbations observed in CIRS maps at the 243-mbar level, but not with structures seen at the 1-mbar pressure level. The highest temperatures near 0° System III longitude correlate with the brightest (UV) region at similar longitude. Such a correlation might be attributed to longitudinally alternating evaporation and condensation of ammonia in the upper troposphere, if the condensed phase is a UV absorber. However, in regions of low aerosol number density, Rayleigh scattering by molecular H_2 and He provides a bright background. Moreover, ammonia ice is a weak absorber in the UV1 filter, so some other mechanism is at work. Photochemically produced hydrazine is likely to be present at the top of the troposphere and may be playing a role. Another possibility is that the UV-absorbing particles are nonvolatile and their concentrations are enhanced by convergence at the crests or troughs of the wave pattern. No wave was visible in the southern hemisphere at comparable latitudes. This lack of symmetry is not unprecedented. For example, the southern hemisphere has more large ovals, and the northern hemisphere has the equatorial plumes (*17*). Presumably, these north-south differences are the result of long-term fluctuations in the zonal winds and cloud bands.

After its closest approach to Jupiter, the Cassini ISS looked back at the dark crescent of the planet and observed the aurora at both the north and south poles (fig. S2). Jupiter's northern auroras on 8, 13, and 20 January 2001 were imaged at a resolution of ~100 km/pixel (*1*). While the Cassini ISS was observing the aurora on the nightside, HST observed the aurora in UV light on the dayside. Our objectives were to compare the brightness in different spectral regions, to compare HST dayside images (*40*) with Cassini nightside images to search for

Table 1. Summary of the Cassini ISS nightside auroral data. The planetocentric latitude of the auroral arc for each 10° of longitude from 150° to 200°W is given. Reference ovals (main and secondary) derived from 82 HST images in UV light on the dayside (*40*) are also shown. Constant longitude lines rotate with the planet at the System III rate defined by the magnetic field. A diurnal effect would show up as a systematic offset in latitude, for the same longitude, between the Cassini data and the HST data. East of 180°W, the Cassini points lie below (to the south of) the HST main reference oval; west of 180°W, the Cassini points lie on top of the HST main reference oval.

Longitude	Date					Reference	
	8 Jan	13 Jan	13 Jan	20 Jan	20 Jan	Main	Secondary
150°W	–	60.4	62.2	61.2	–	–	–
160°W	55.6	55.5	56.6	56.4	56.0	57.4	54.6
170°W	55.0	55.9	55.4	55.5	55.2	56.1	53.9
180°W	56.6	57.0	56.6	57.2	–	56.9	55.1
190°W	59.0	–	58.8	–	–	58.9	57.7
200°W	61.8	–	62.5	–	–	61.4	61.0

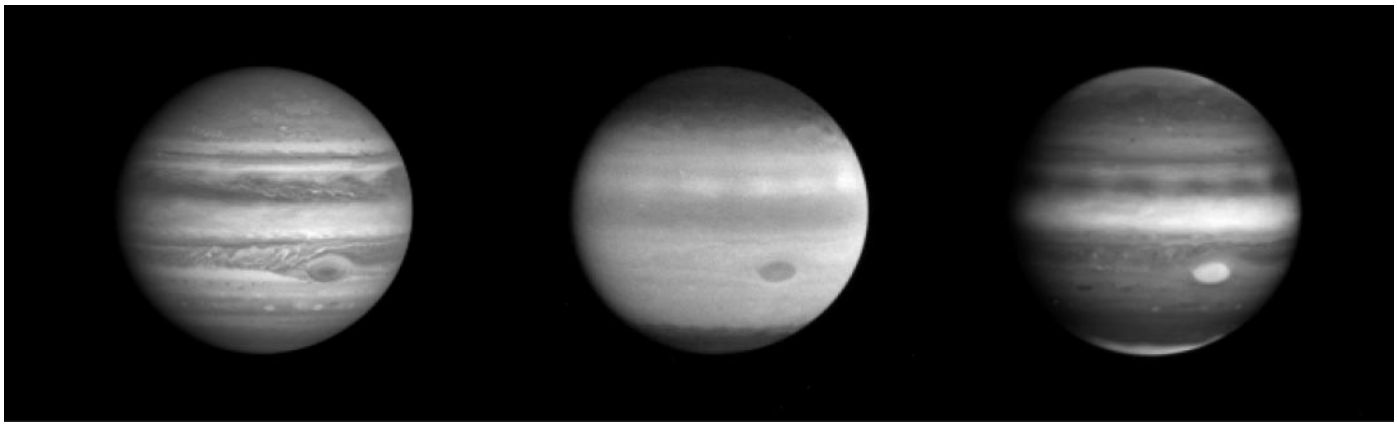

Fig. 5. Three images of Jupiter (**left**) in blue (451 nm), (**middle**) in UV (258 nm), and (**right**) in the strong methane band (889 nm). A wave pattern, which circumnavigates the globe, is easily seen near 14°N latitude in both UV and methane images. It seems to be correlated with waves in the clouds seen at the same latitude in the blue image.

diurnal changes, and to look for changes over a 12-day period with Cassini data (table S1) and over a 4-year period with Cassini and Galileo data (*41, 42*).

The Cassini nightside observations lie below (to the south of) the HST main reference dayside oval (at least east of 180°) (Table 1), consistent with the idea (*40*) that the magnetosphere, and therefore the auroral oval, expands on the nightside and contracts on the dayside in response to the variation in solar wind pressure between day and night (*43, 44*). In general, the Galileo data from 4 years earlier exhibit the same behavior. However, the Galileo and Cassini observations of the auroral oval do not always coincide with each other (Fig. 6). The Galileo points lie 1° south of the Cassini points at some longitudes, including those between 150° to 180°W longitude, where Cassini data are most reliable. We conclude that the aurora changes on time scales of several years or less. Moreover, the Cassini data are not always coincident with each other. Auroral measurements taken 10.5 hours apart on the same day, 13 January 2001, differ in their relative positions on the planet. The earlier auroral observations lie inside (to the north of) the later observations west of the 170°W meridian, but they lie to the south of the later observations east of the 170°W meridian. The difference is larger than the error bar, so it is significant. These temporal changes recorded by Cassini on the nightside are consistent with those seen on the dayside (*40*). They could be a response to temporal changes in solar wind pressure, or they could arise spontaneously in Jupiter's magnetosphere. They could also reflect changes with respect to local time of day, because the earlier data were taken when the 170°W meridian was closer to the terminator and farther from the midnight meridian.

Satellites and rings. Cassini captured several time-lapse image sequences of Io, Europa, and Ganymede being eclipsed by Jupiter (*1*). Atmospheric emissions were detected from both Io and Europa; none were detected from Ganymede. Io's emissions were detected in previously unseen spectral regions, from 250 to 380 nm and from 670 to 850 nm. During an eclipse on 1 January 2001, Io crossed the plasma torus center as it passed through System III magnetic longitudes from 250° to 303°. Equatorial glows, which shifted in latitude during this 2-hour eclipse, were observed in the visible, tracking the tangent points of the jovian magnetic field lines as the event progressed (fig. S4 and movie S3). This behavior is similar to that observed for UV and other atomic emissions [e.g., (*45*)] and confirms that the visible glows are also powered by the cooling of torus electrons that, constrained to move along the planet's magnetic field, have convected into Io's atmosphere and interact with the neutral species there (*46*). An eclipse on 5 January 2001 provided the best spectral measurements of these glows, which were detected at intensities of ~100 kilorayleighs (kR) or less in UV2 (298 nm), UV3 (338 nm), and BL1 (451 nm) filters. A detection of the equatorial glows was made in the IR1 band (670 to 850 nm), possibly due to singly ionized oxygen ([O II] 732,733 nm). The ultraviolet (UV3) emissions, between 300 and 380 nm, are restricted to the deep atmosphere near the surface of Io, whereas the red glows are much more extensive (reaching

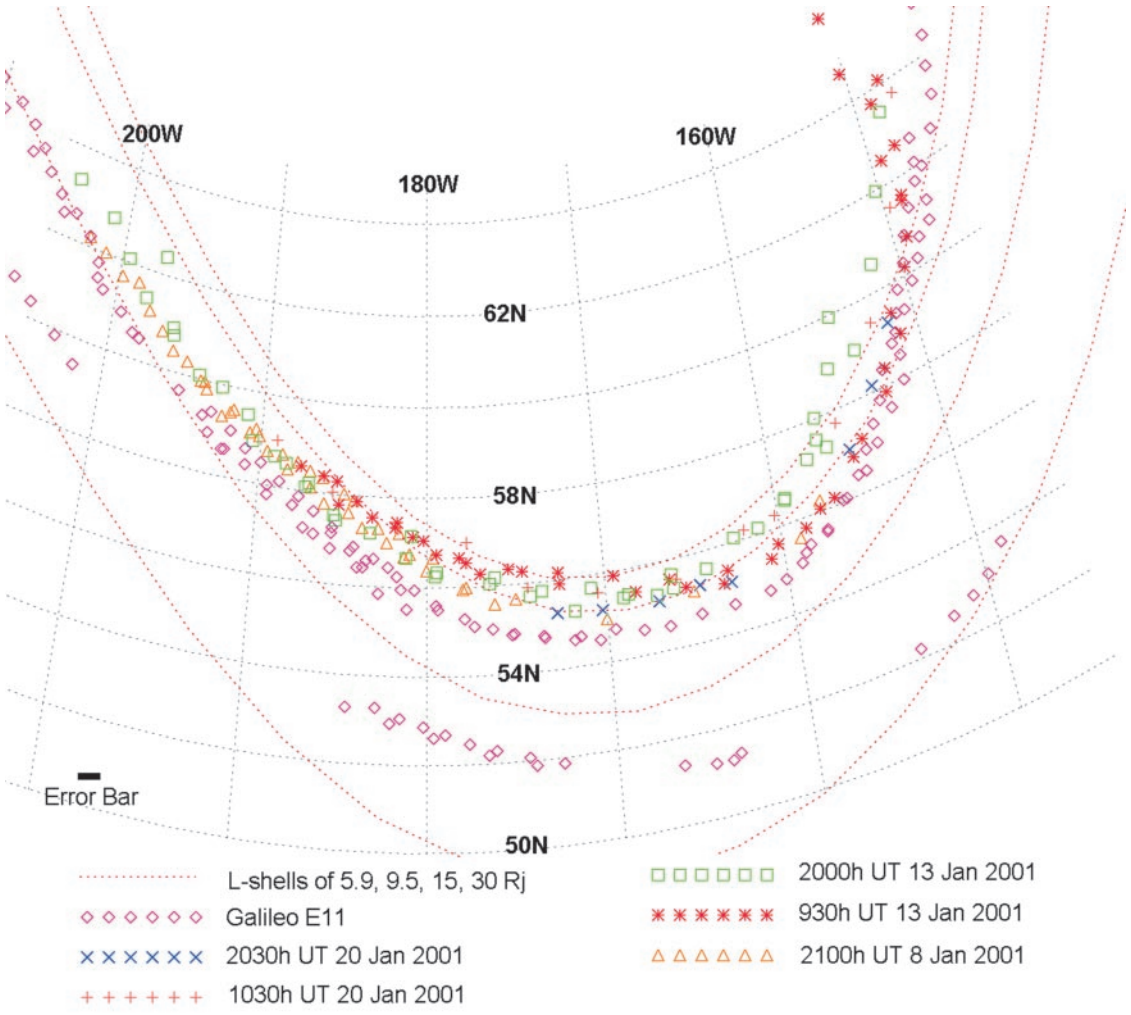

Fig. 6. Jupiter's primary northern auroral arc as observed by Cassini in System III planetary coordinates (planetocentric latitude and west longitude). The error bar is the projection of a line 2.5 pixels long at ~160°W onto the horizontal plane. Different colors correspond to different times of observation. The Cassini data are shown for 8, 13, and 20 January 2001. The aurora as observed by Galileo on orbit E11 is shown as a set of purple diamonds (*41*); the dashed lines are L shells corresponding, from south to north, to 5.9, 9.5, 15, and 30 R_J, as predicted by the VIP4 magnetic field model (*69*). (An L shell is a three-dimensional surface defined by magnetic field lines that cross the equatorial plane at a particular radial distance from the planet's center. Here we indicate where they intercept the surface of the planet.) The HST main reference oval lies close to the 30 R_J L shell. The difference between the longitude of the Sun and the longitude of a point on the aurora is a measure of the local time of day. Camera pointing reconstruction is obtained from stars in the image to an accuracy of 1 to 2 pixels, and the aurora is measured to 1 to 2 pixels; the error bar represents a band of width 1σ for our measurements. The error increases to the west because there is more scattered light from the bright crescent; the error also increases to the east because the aurora goes over the limb in most of the images.

heights of up to 900 km). This would be expected if the UV glows are produced by sulfur dioxide, which is heavier than atomic oxygen and more closely bound to the surface by Io's gravity, whereas the red emissions may arise from a tenuous atmosphere of atomic oxygen.

Europa's visible emissions had been detected by other means but had not been resolved (*47*–*50*). Cassini's spatially resolved images of Europa in eclipse showed that its visible auroras, like the UV oxygen emissions observed by the Space Telescope Imaging Spectrograph of HST (*51*), are brightest around the limb of the satellite, indicating an atmospheric rather than surface source (fig. S5). Neutral oxygen and/or sodium emissions of ~10 kR could explain the observed brightness.

Cassini images of Io revealed two giant plumes: Pele, a 400-km-high equatorial plume discovered by Voyager, and a previously unseen plume over the north pole (fig. S6). The two plumes have similar spectral properties, consistent with those reported previously for Pele (*52*). After the acquisition of joint Galileo images, we recognized that the vent for the north polar plume was Tvashtar Catena, located at 63°N latitude on the opposite side of Io as seen by Cassini. Cassini imaged only the top of the plume, which must be ~400 km high. (A concentration of emissions near the north pole of Io was seen in all three Io eclipses and was most likely caused by the plume erupting from the Tvashtar volcano.) These observations by Cassini, supported by others obtained late in the Galileo extended mission, confirm a class of large but short-lived plumes at high latitudes (*53*), associated with voluminous outpourings of lava, possibly indicating tidal heating in Io's deep mantle as the cause.

Cassini obtained disk-resolved images of Himalia, an outer satellite of Jupiter (Fig. 7) (*1*). The measured size range of Himalia, taken from a distance of 4.44 million km and an image scale of 27 km/pixel, is 4 to 6 narrow-angle pixels, indicating an irregular shape that is not dominated by gravity. These values correspond to radii of 75 ± 10 km by 60 ± 10 km, if the principal axes (or dimensions close to them) were measured (*54*), and are close to the mean ground-based radius of 85 km (*55*). The surface albedo, scaled from the ground-based flux measurements and the new size determination, is 0.05 ± 0.01, which, together with the gray color (*56*), is consistent with a C-type (carbonaceous) asteroidal surface and a possible capture origin for Jupiter's outer prograde satellites.

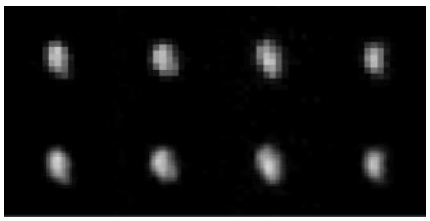

Fig. 7. The disk of Himalia illuminated from the left at a phase angle of 70° and observed by the Cassini ISS over ~4.5 hours. One unprocessed image, taken through the BL1 (451 nm) filter, from each of four observation sequences is shown in the top row. The observation UTC times were (from left to right) 18 December 2000, 20:30, 22:00, and 23:30, and 19 December 2000, 01:04. The bottom row shows the same data, but smoothed by bicubic interpolation.

The small inner jovian satellites Metis and Adrastea were imaged between early December 2000 and mid-January 2001, and the results were used to improve knowledge of their orbits (Table 2) (*1*). These results are consistent with those from previous observations (*57, 58*), with the notable exception that we are now able to measure statistically significant inclinations. To within 2σ, the satellites' inclinations are identical to each other and imply a maximum vertical displacement from the jovian equatorial plane of ~100 km. These results establish with confidence that either one or both of these bodies are, in part, the sources of the jovian main ring (*59, 60*) and that their inclinations determine the ring's vertical thickness (*57, 61, 62*). The source of these inclinations is at present unknown, although resonance passage by Io (*63*) early in the history of the jovian system may be a cause.

During Cassini's approach to Jupiter, from 4 October to 6 December 2000, 160 NAC images were taken to search for any undiscovered satellites of Jupiter, focusing (to avoid scattered Jupiter light) on the region exterior to Amalthea but interior to Callisto (*1*). At present, we are confident that no satellites exist between 2.6 and 20 R_J with inclinations of <1.6°, eccentricities of

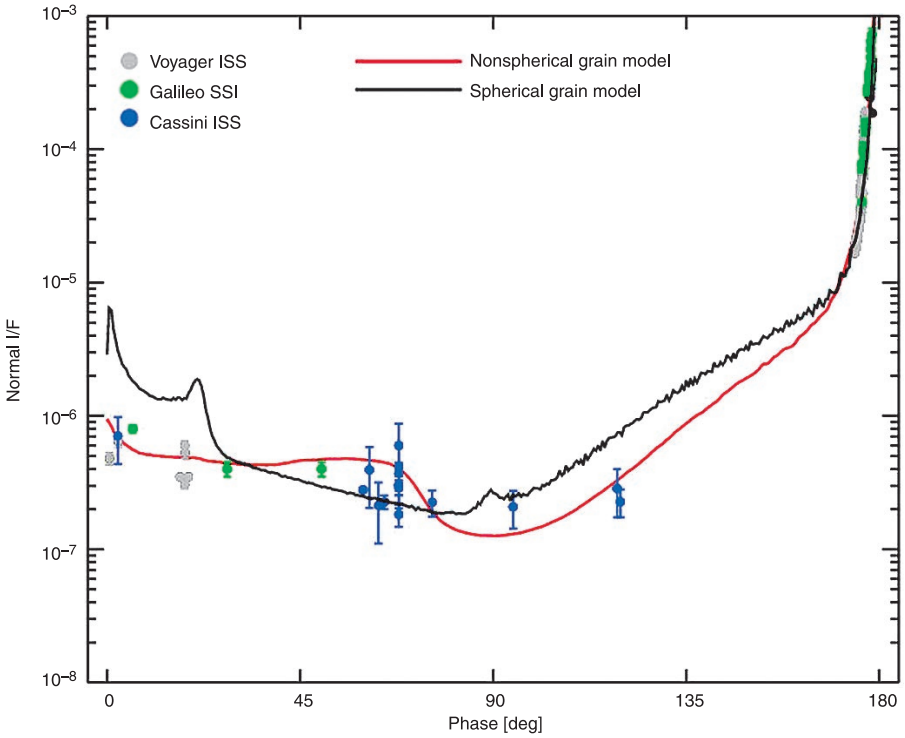

Fig. 8. The phase behavior of the jovian main ring at visible wavelengths over the range of observed phase angles. All values are in units of I/F as observed normal to the ring plane at the observed phase angle (where I is the measured intensity, and πF is the solar flux incident on the ring planes). The Cassini ISS data are plotted along with data from the Voyager imaging experiment (*61*) and the Galileo Solid-State Imaging instrument (*64, 65*). Best fitting nonspherical and spherical grain models (as described in the text) are indicated.

Table 2. Geometrical orbital elements for Metis and Adrastea [epoch 2451891.0 JED (Julian ephemeris date)]. Longitudes were measured from the intersection of the ascending node of the jovian equatorial plane on the Earth mean equator at epoch in J2000. Errors are formal 1σ uncertainties.

Element	Metis	Adrastea
Semi-major axis, *a* (km)	127,979.8 ± 0.1	128,980.5 ± 0.1
Mean longitude, λ (°)	80.13 ± 0.03	235.95 ± 0.05
Mean motion, *n* (°/day)	1221.252 ± 0.001	1207.001 ± 0.001
Eccentricity, *e*	0.0002 ± 0.0001	0.0015 ± 0.0009
Longitude of pericenter, ϖ(°)	110 ± 30	98 ± 12
Inclination, *i* (°)	0.06 ± 0.01	0.03 ± 0.01
Longitude of ascending node, Ω (°)	196 ± 5	191 ± 25
RMS error (arc sec)	0.7	0.9

<0.0002, and visual magnitudes (as seen from a range of 40 million km) brighter than 14.5. The latter limit corresponds to an object with a diameter of 15 km and an albedo of 0.1.

Cassini images of the jovian main ring sampled a broad range of wavelengths and viewing geometries over a period of 37 days during the flyby (fig. S7). The analysis of the clear-filter images, in combination with results from Voyager and Galileo image analyses (*61, 64, 65*), produced a new ring phase curve (Fig. 8). Cassini images fill in broad holes in the ring's phase coverage, in particular 60° to 120°, a range that can be diagnostic of nonspherical particles.

Using a nonspherical particle model, we fit the ring's phase curve with two components: (i) large parent bodies having a geometric albedo of 0.063 [similar to that of Metis (*66*)] and a Callisto-like phase function, and (ii) small nonspherical grains (*67*) with a power law size distribution index of $q = 2$ in the size range of 0.01 to 15 μm and an index of $q = 5$ for particles that are >15 μm. For comparison, we also applied a two-component model consisting of large bodies and spherical Mie-scattering grains from 0.01 to 100 μm (Fig. 8). The nonspherical model yields a better fit to the data than do spheres, in particular because of a generally flatter low- to mid-phase behavior for such grains. However, it produces the same normal optical depth τ of large bodies ($\tau_l \sim 3 \times 10^{-6}$) and small grains ($\tau_s \sim 2 \times 10^{-6}$) as do previous two-component models that rely on small Mie scatterers, with a notable concentration of surface area in grains that are ~15 μm in size. We favor the nonspherical particle model, which is more consistent with the traditional view that erosive micrometeoroid impacts into Metis, Adrastea, and the large ring bodies are the source of the dust component, although a process for enhancing the population of 15-μm particles is not currently known.

References and Notes

1. See supporting data on *Science* Online.
2. C. C. Porco *et al*., in preparation.
3. From 11 to 13 December 2000, the ISS acquired a 1 × 2 mosaic every hour for 38 hours, producing 29 pairs of images, each separated from the other by one planetary rotation (10 hours). Wind measurements were taken from these image pairs. Spatial resolution ranged from 122 to 114 km/pixel, resulting in a wind speed precision of ~3.3 m/s. Images were navigated on the planetary limb, calibrated radiometrically, assembled into spatial mosaics, and mapped with a simple cylindrical projection. Illumination effects were removed by dividing the brightness values by the cosine of the solar incidence angle. Zonal winds were measured with an automatic line-shifting method. Each map line spans 0.1° latitude (~1250 km). Because blocks of five lines were shifted and digitally correlated, the latitudinal resolution of our zonal velocity profile is 0.5°.
4. S. S. Limaye, *Icarus* **65**, 335 (1986).
5. A. R. Vasavada *et al*., *Icarus* **135**, 265 (1998).
6. A. A. Simon, *Icarus* **141**, 29 (1999).
7. E. Garcia-Melendo, A. Sanchez-Lavega, *Icarus* **152**, 316 (2001).
8. A. P. Ingersoll, C. C. Porco, *Icarus* **35**, 27 (1978).
9. F. H. Busse, *Icarus* **29**, 255 (1976).
10. A. P. Ingersoll, D. Pollard, *Icarus* **52**, 62 (1982).
11. R. L. Kirk, D. J. Stevenson, *Astrophys. J.* **316**, 836 (1987).
12. We imaged in a continuum spectral region (751 nm) sensitive to clouds at all levels down to great depth, a weak methane absorption band (727 nm) sensitive to somewhat higher cloud tops, and a strong methane band (889 nm) that detects clouds with tops in the upper troposphere (*18*). Localized regions that are bright at all three wavelengths have high-altitude tops and are optically thick. Similar features in terrestrial satellite images are vertically extensive and associated with deep moist convective instability (*68*). A similar Galileo feature was collocated with a previous lightning detection and identified as convection (*19*). To confirm our storm identifications and to ensure that no other events were missed, we examined scatter plots of the weak methane band versus continuum brightness for both the small region containing the feature (compare fig. S1) and the large-scale region excluding the convective area. Features with high-continuum albedo (i.e., optically thick clouds) and anomalously high brightness in the weak methane band (i.e., high cloud tops) were identified as convective storms.
13. Latitudinal shear of the zonal wind is characterized as cyclonic or anticyclonic according to the sense of rotation that would be induced in an object placed into the flow. Cyclonic shear corresponds to counterclockwise rotation in the northern hemisphere and clockwise rotation in the southern hemisphere, as is found poleward of the eastward jets. The opposite sense of rotation defines anticyclonic flow.
14. One hundred fifty-six candidate storms were identified in images spanning 1 to 15 December 2000 and 29 December 2000 to 7 January 2001, during which NAC image scale varied from ~60 to 175 km/pixel. Images were obtained for ~67% of the available time pre-encounter and ~20% near- and post-encounter, equivalent to ~12 continuous days of global imaging. Removing multiple observations of the same storm at different times reduced the number of storms to 64 independent candidates, and an examination of scatter plots of albedo in the three channels eliminated some questionable features, resulting in 43 high-confidence separate storm identifications.
15. W. J. Borucki, J. A. Magalhaes, *Icarus* **96**, 1 (1992).
16. B. Little *et al*., *Icarus* **142**, 306 (1999).
17. B. A. Smith *et al*., *Science* **204**, 951 (1979).
18. D. Banfield *et al*., *Icarus* **135**, 230 (1998).
19. P. J. Gierasch *et al*., *Nature* **403**, 628 (2000).
20. A. D. Del Genio, K. B. McGrattan, *Icarus* **84**, 29 (1990).
21. R. Hueso, A. Sanchez-Lavega, *Icarus* **151**, 257 (2001).
22. B. E. Carlson, A. A. Lacis, W. B. Rossow, *J. Geophys. Res.* **99**, 14623 (1994).
23. P. G. J. Irwin, U. Dyudina, *Icarus* **156**, 52 (2002).
24. E. J. Zipser, K. R. Lutz, *Mon. Weather Rev.* **122**, 1751 (1994).
25. A. D. Del Genio, W. Kovari, *J. Clim.* **15**, 2597 (2002).
26. J. A. Pirraglia *et al*., *Nature* **292**, 677 (1981).
27. M. Allison, *Planet. Space Sci.* **48**, 753 (2000).
28. A. P. Ingersoll *et al*., *Nature* **403**, 630 (2000).
29. B. A. Albrecht *et al*., *Bull. Am. Meteorol. Soc.* **76**, 889 (1995).
30. Molecular scattering by H_2 and He and scattering and absorption by aerosols are important opacity sources in the UV. Absorption by ammonia or acetylene averaged over the spectral band between 250 and 280 nm is negligible in comparison to that from aerosols. Consequently, we assumed that jovian absorption in the near-UV is attributable to aerosol particles. (A broad gaseous molecular absorption may also be important. If so, its composition is unknown.)
31. A. Sanchez-Lavega, R. Hueso, J. R. Acarreta, *Geophys. Res. Lett.* **25**, 4043 (1998).
32. M. B. Vincent *et al*., *Icarus* **143**, 205 (2000).
33. Several HST images were used to measure polar stratospheric winds, and differences were found when these winds were compared to tropospheric winds (*32*). A UV-dark oval was found near planetocentric latitude 60°N, having about the same size and shape as Jupiter's Great Red Spot in an HST image obtained in 1997 with a filter having the same spectral characteristics as the UV1 filter on the ISS NAC. It was not seen in other UV images from HST, which were taken on average once or twice per year between 1994 and 1999, although not all images have been examined closely. Therefore, before the Cassini encounter, it was thought that this type of feature was rare or perhaps a singular event.
34. S. W. H. Cowley, E. J. Bunce, *Planet. Space Sci.* **49**, 1067 (2001).
35. R. A.West, *Icarus* **38**, 12 (1979).
36. M. B. Vincent *et al*., *Icarus* **143**, 189 (2000).
37. A. P. Ingersoll *et al*., *Nature* **280**, 773 (1979).
38. G. S. Orton *et al*., *Science* **265**, 625 (1994).
39. F. M. Flasar *et al*., in preparation.
40. J. H. Waite Jr., personal communication.
41. A. P. Ingersoll *et al*., *Icarus* **135**, 251 (1998).
42. A. R. Vasavada *et al*., *J. Geophys. Res.* **104**, 27133 (1999).
43. D. A. Gurnett *et al*., *Nature* **415**, 985 (2002).
44. W. S. Kurth *et al*., *Nature* **415**, 991 (2002).
45. F. L. Roesler *et al*., *Science* **283**, 353 (1999).
46. D. Strobel, personal communication.
47. D. Hall, D. Strobel, P. Feldman, M. McGrath, H. Weaver, *Nature* **373**, 677 (1995).
48. M. Brown, R. Hill, *Nature* **380**, 229 (1996).
49. Hall and others (*47*) observed atomic O emissions in the extreme UV, and Brown and Hill (*48*) detected extended visible emission in Na D lines.
50. C. Hansen *et al*., in preparation.
51. M. McGrath *et al*., paper presented at the 32nd Annual Meeting of the Division of Planetary Sciences, American Astronomical Society, Pasadena, CA, 23 to 27 October 2000.
52. J. R. Spencer *et al*., *Geophys. Res. Lett.* **24**, 2471 (1997).
53. A. S. McEwen, L. A. Soderblom, *Icarus* **55**, 191 (1983).
54. T. Denk *et al*., paper presented at the conference on Jupiter: The Planet, Satellites, and Magnetosphere, Boulder, CO, 25 to 30 June 2001.
55. D. P. Cruikshank, *Icarus* **30**, 224 (1977).
56. J. Degewij *et al*., *Icarus* **44**, 520 (1980).
57. M. E. Ockert-Bell *et al.*, *Icarus* **138**, 188 (1999).
58. R. A. Jacobson, personal communication.
59. J. A. Burns, M. R. Showalter, J. N. Cuzzi, J. B. Pollack, *Icarus* **44**, 339 (1980).
60. E. Gruen, G. Morfill, G. Schwehm, T. V. Johnson, *Icarus* **44**, 326 (1980).
61. M. R. Showalter, J. A. Burns, J. N. Cuzzi, J. B. Pollack, *Icarus* **69**, 458 (1987).
62. The best measurement of jovian main ring thickness is that estimated from high-resolution Galileo images: ~100 km at a phase angle of ~90° (*57*). Voyager placed an upper limit on the ring's thickness seen in forward-scattered light (presumably the fine dust component) of 300 km (*61*). Small dust particles are brightest in forward scattering, whereas larger particles are brightest in back-scattered light; therefore, it is possible that the small particles have a different vertical distribution than the large particles.
63. D. P. Hamilton, A. L. Proctor, K. P. Rauch, *Bull. Am. Astron. Soc.* **33**, 1085 (2001).
64. M. R. Showalter *et al*., paper presented at the conference on Jupiter: The Planet, Satellites, and Magnetosphere, Boulder, CO, 25 to 30 June 2001.
65. S. M. Brooks, L. W. Esposito, M. R. Showalter, H. B. Throop, in preparation.
66. P. Thomas *et al*., *Icarus* **135**, 360 (1998).
67. M. I. Mishchenko, L. D. Travis, *J. Quant. Spectrosc. Radiat. Transfer* **60**, 309 (1998).
68. R. Fu, A. D. Del Genio, W. B. Rossow, *J. Clim.* **7**, 1092 (1994).
69. J. E. P. Connerney, M. H. Acuna, N. F. Ness, T. Satoph, *J. Geophys. Res.* **103**, 11929 (1998).

70. We gratefully acknowledge the assistance of many individuals in planning and executing the imaging science investigation during the Cassini Jupiter flyby, in particular D. Dawson, K. Grazier, C. Hansen, V. Haemmerle, B. Janes, D. Lytle, and E. McCartney. We also acknowledge the financial support of Cosmos Studios in the creation of atmospheric movies from the Jupiter flyby.

Supporting Online Material

www.sciencemag.org/cgi/content/full/299/5612/1541/DC1
SOM Text
Figs. S1 to S7
Table S1
Movies S1 to S4

16 October 2002; accepted 21 January 2003